Immuno-polymer lipid nanoparticles for delivery and protein expression in cells

Arvind K. Jain[1, 3], Carole Bataille[2],
Sabine Milhas[1], Ami Miller[1], Jing Zhang[1], Terry H. Rabbitts[1]

1. Weatherall Institute of Molecular Medicine, MRC Molecular Haematology Unit, University of Oxford, John Radcliffe Hospital, Oxford, OX3 9DS, UK

2. Chemistry Research Laboratory, University of Oxford, 12 Mansfield Rd, Oxford OX1 3TA, UK

3 Current address: Sun Pharma Advanced Research Company Ltd., Sun Pharma Road, Tandalja, Vadodara- 390012, INDIA

Key words: mRNA delivery, cytosolic delivery, Polymer Nanoparticles, PLA-PEG, macromolecule delivery, CD7, T-ALL

Running title: Polymer-Lipid nanoparticles encapsulating mRNA for cellular delivery

Corresponding author: Terry Rabbitts, Weatherall Institute of Molecular Medicine, MRC Molecular Haematology Unit, University of Oxford, John Radcliffe Hospital, Oxford, OX3 9DS, UK terence.rabbitts@imm.ox.ac.uk

Abstract

Macromolecules such as antibody fragments (herein called macrodrugs) have been reported that can interfere with intracellular targets but their use is limited to delivery systems where expression is achieved from vectors such as plasmids or viruses. We have developed homogeneous poly-lactic acid PEGylated nanoparticles, and including the cationic lipid 1,2-dioleoyl-3-trimethylammonium-propane (DOTAP), that are functionalized with monoclonal anti-CD7 antibody for receptor-mediated endocytotic delivery of macrodrug mRNA. Similarly, antigen-specific endocytosis was produced in T cell leukaemia cell lines using nanoparticles functionaliszed with anti-CD53 or anti-GPR56 antibodies. Incorporation of DOTAP as the lipid component of the poly-lactic acid nanoparticles enhanced release of the immuno-particles from the endosomes following cell entry for release of reporter mRNA into the cytosol compared to NPs from poly-lactic acid alone. Systemic delivery of these anti-CD7 immuno-nanoparticles into humanised CD7 transgenic mice, resulted in localisation in the spleen, uptake into splenocytes and release of low amounts of reporter mRNA translation. These functionalised nanoparticles are the basis for elaboration and optimisation for realising their potential in therapeutic applications to carry specific macrodrug mRNAs targeting intracellular proteins mediating diseases.

Introduction

Drug development in recent years has begun to focus on targeted therapy where the chemical drug interferes with specific properties of a protein. Notable successes have been in compounds that inhibit the kinase activity of the chromosomal translocation proteins BCR-ABL [1, 2] or BRAF inhibition drugs [3, 4]. An alternative strategy is the selection of macromolecular protein inhibitors that can more readily be produced with enhanced potency using molecular biology techniques. These include antibody fragments [5, 6], peptide aptamers [7, 8] and peptides [9]. In addition to the importance of selection techniques, protein drugs (herein called macrodrugs [10]) can perform functions such as inhibiting protein-protein interactions which have been thought to be more challenging to target with small molecules [11] but also to be capable of drugging previously undruggable targets like mutant RAS [12] or transcription factors [13].

One of the problems with the use of macromolecules as macrodrugs is that proteins generally do not enter cells unless they first bind to a receptor on the surface, for example like antibodies bind to cell surface proteins, and subsequently internalized by endocytosis. Protein transduction has been well developed in which small peptide elements, such as from Antennapedia [14] or HIV tat elements [15, 16], have been appended to proteins or fragments. Nonetheless, apart from immunogenicity issues, proteins are physicochemically diverse and may be degraded if administered systemically preventing them from reaching their target location. Ideally, methods are required to deliver macrodrugs to cells in protected form, prior to their being released into the cytosol.

Potentially, genetic material (DNA or RNA) encoding for macrodrugs is an alternative delivery option. DNA delivery has been achieved with viral and non-viral vectors [17-20] but also mRNA because it can be directly translated to the protein of interest in the cytosol by the translation machinery of the [21-23] cell. Chemical modifications of synthetic mRNA renders it more efficiently translated, making mRNA

a feasible candidate as a therapeutic agent [24-26] but degradation after systemic administration before reaching its molecular target is a factor that leads to inefficient utility. Protection of systemically delivered nucleic acid using attenuated viruses has been developed but these have limitations of safety and complicated manufacturing processes adding potentially high costs of goods. On the other hand, non-viral systems based on variety of polymers and lipids have shown promise [27-30] and are currently the lead non-viral delivery system for nucleic acids, with FDA approved formulations [31].

Lipid nanoparticles (LNPs) and polymeric nanoparticles, such as comprising biodegradable poly-lactic acid (PLA) have been used for encapsulation of RNA [32, 33] and some are in clinical trials to deliver siRNA and shRNA, along with Onpattro® that is an FDA approved siRNA LNP-based commercial product by Alnylam Pharmaceuticals [34-37]. Like siRNA, mRNA also needs to cross the barrier of cell membranes to reach the intracellular space, and also requires protection from extracellular ribonucleases that are present in blood. Safe homing of mRNA within nanoparticles has shown promising results for protein synthesis from the mRNA cargo [38, 39] but there are limited numbers of reports. We have recently described a novel LNP formulation able to encapsulate mRNA and delivery this mRNA for protein translation to a variety of cells, but mRNA release requires enhancement by the application of shock waves [40].

There are several general problems with mRNA delivery. First, achieving sufficient mRNA loading within the particles so that reasonable levels of protein can be produced following cellular uptake of the NPs and release of the mRNA and second, selectivity towards the desired target cell. The poly-lactic acid-based NPs can potentially overcome these problems [41, 42] since these are formed by double emulsion solvent evaporation where nucleic acid is encapsulated in the internal water droplet, which condenses the nucleic acid material to smaller cores in the polymer matrix bed during the evaporation step. Including positively charged DOTAP further

assists condensing negatively charged nucleic material and reduces the chances of their escape from internal aqueous phase to external phase during the polymer hardening process leading to efficient encapsulation [33]. Further, the application of functionalised NPs, in which monoclonal antibodies are linked to the coat of the NPs (immuno-nanoparticles), can potentially address the limitation of non-selective delivery of the NPs because cell surface-binding antibodies provide specificity along with rapid receptor-mediated endocytosis [43, 44]. In this respect, the surface protein CD7 is of particular interest for our work on T cell acute leukaemia (T-ALL). This protein is expressed on all T-ALL as well as a proportion of acute myeloid leukaemias and can be internalised by binding anti-CD7 antibody [45].

We have developed immuno-polymeric lipid composite nanoparticles made from PEGylated PLA and the cationic surfactant DOTAP generating nanoparticles with co-polymer of hydrophobic poly-lactic acid, covalently conjugated to a hydrophilic chain of PEG. An anti-CD7 monoclonal antibody has been functionalized to the NP surface and mRNA encapsulated in the PLA that forms the core of the NPs acting as a reservoir for the cargo, DOTAP improves release of the NPs from endosomes to allow some mRNA release after exposure to the low endosomal pH and membrane fusion. We demonstrate that these immuno-particles, functionalised with anti-CD7 antibody, preferentially engage CD7-expressing cells *in vitro* and *in vivo*.

Results

Immuno-nanoparticle characterisation

Nanoparticles were synthesized with PLA-PEG block copolymers of various chain lengths and the polylactic acid and polyethylene glycol were covalently conjugated to give a single polymeric chain. Pre-formed PEG of various sizes (Mw 2000, 3400 and 5000 Da) was used and lactide monomers were polymerized to obtain a chain length ratio of 4:1 of lactide monomers:ethylene glycol. PLA forms a hydrophobic core of the nanoparticles and is mainly responsible for carrying the cargo (in our work mRNA) and for controlling their release profile, whereas PEG forms the corona around the nanoparticles and gives a structure around the spherical core [46].

Since the PEG chains are the primary interfaces seen by the cells, they confer the interaction behavior of the nanoparticles with the cells and the longer chain lengths have a higher repulsion by cells. Block copolymers were synthesized by ring opening polymerization (ROP) with various PEGs (2000, 3400 and 5000Da). ^{1}H-NMR confirmed the synthesis of the copolymer and their chain lengths (Supplementary Figure S1). Nanoparticles were generated by double emulsion solvent evaporation method [Jain 2015]. The formulation method was optimized for empty nanoparticles prepared with molecular weight 3400 Da for process variables that generated uniform nanoparticles of 156±4 nm (Table 1) and this method was subsequently implemented for other copolymers for the synthesis of nanoparticles.

For the conjugation of the antibodies on the surface of the nanoparticles, PLA-PEG-maleimide was used and freshly prepared NPs were incubated with thiolated antibodies (treated with Traut's reagent) at room temperature in PBS. The average hydrodynamic diameter of the immuno-nanoparticles (i-NPs) was found to be 171 ±6nm (Table 1). The presence of antibodies on the surface of NPs caused a slight decrease in the zeta potential of the i-NPs compared to NPs. Nanoparticles prepared with PLA-PEG2000 and PLA-PEG5000 showed a similar trend where antibody conjugated i-NPs displayed slightly higher averaged diameter than the

native non-conjugated NPs. Further, these nanoparticles had enlarged diameter with increase in the polymer molecular weight as this provides longer PLA chains to form the core of the NPs and giving it the bulk.

Lipid composite NPs were formulated of PLA-PEG3400 polymers, in which 5 or 10% w/w polymer was substituted by DOTAP. This was found to decrease the particle size (perhaps by causing a denser core), and decrease in zeta potential that may be attributed to the positive charge of DOTAP (Table 1). The presence of the positive charged lipid in the polymer phase also ensured the better encapsulation of mRNA and retention during the solidification step of solvent evaporation.

The PEG chains form the corona around the nanoparticles that prevents adsorption of the proteins to the surface of circulating NPs giving them longer blood circulation half-life [47, 48] as well as potentially avoiding non-specific uptake by cells. The cell-association of NPs or i-NPs was assessed in culture with the human T cell lines Jurkat and KOPT-K1 (both expressing the surface protein CD7 (Supplementary Figure S2)) using fluorescently-labelled NPs and flow cytometry. This shows that PEG2000 was not efficient to avoid the non-specific adhesion of NPs to the surface of Jurkat and KOPT-K1 (Figure 1A, C), while nanoparticles with PEG3400 or PEG5000 exhibited low levels of non-specific association with these cells. In addition, while PEG is required to avoid non-specific uptake, it does not interfere with receptor mediated endocytosis since anti-CD7 antibody conjugated nanoparticles showed significant uptake by both lines for all three PEG lengths (Figure 1B, D).

i-NPs specifically bind to CD7 positive cells

For further evaluation of the specificity of PLA-PEG3000, the CD7 expressing human T cell lines (Jurkat, KOPT-K1 and MOLT4, Supplementary Figure S2) and various CD7 negative cells (the mouse myeloma NS0, the human Burkitt's lymphoma RAJI and murine erythro-leukaemia MEL cells) were incubated with PLA-PEG3000 i-NPs

and were evaluated for the uptake by flow cytometry analysis (Figure 2A, B). None of the CD7 negative cells showed any association with the PLA-PEG3000 i-NPs or NPs, whereas all three CD7 expressing cells showed a good uptake of i-NPs (Figure 2A).

The requirement for expression of surface CD7 was further assessed using an engineered derivative of the human lung carcinoma cell line A549 that expresses surface CD7 (herein A549-CD7 cells) (Supplementary Figure S2B). In the same way as naturally CD7 expressing cell lines, the A549-CD7 cell line exhibited specific uptake of i-NPs only (Figure 3A, B) whereas A549 parental cells (CD7-negative) did not display association with i-NPs on their surface (Figure 3B). The specificity was confirmed by seeding mixtures of A549-CD7 cells together with native A549 cells ($CD7^-$) at various ratios and incubating with fluorescent NPs. After four hours, cells were recovered and analysed by flow cytometry with anti-CD7 antibody, thereby comparing cell numbers with surface CD7 labelling with NP uptake (fluorescent particles). A high percentage of A549-CD7 cells take up the i-NPs (Figure 3C) and when mixed populations of A549-CD7 with A549 were transfected, the fraction of positively transfected A549-CD7 cells in the seeded populations was reflected by the proportion of i-NPs positive cells (Figure 3D, E).

i-NPs could be made by conjugating with other antibodies that define specific cell surface proteins. I-NPs were prepared with anti-CD53 or anti-GPR56 antibodies and these were tested on KOPT-K1 cells (cells that naturally express CD53 and GPR56) along with CD7 antibody. Each of the specific i-NPs bound to these T cells, albeit with varying levels of association. Unconjugated NPs showed no association with the cells (Supplementary Figure 3A).

Modified mRNA encapsulated PLA-PEG NPs

Our purpose was to develop NPs that could encapsulate mRNA, carry the molecules safely to cells, and release the mRNA in an intact form for protein translation. The

substitution of pseudo-uridine for uridine during the *in vitro* transcription mRNA helps it evade recognition and cleavage by ribonuclease [25] and avoids recognition by Toll-like receptors as well as by retinoid-inducible gene I (RIG I) [24, 49, 50], and it does not activate protein kinase PKR [26, 51]. Accordingly, we synthesized modified EYFP reporter mRNA and initially tested this by lipofectamine-mediated transfection compared to unmodified mRNA (Supplementary Figure S4). Fluorescence microscopy images (panels A-D) indicate that the modified mRNA is superior in the translational capacity than normal synthesized mRNA and the EYFP fluorescence intensity increases with mRNA dose dependency (panel E, F). To ensure the nanoparticle preparation did not affect the physical or biological stability of the mRNA, the nanoparticle-encapsulated mRNA was extracted by disrupting the NPs in chloroform:water where chloroform dissolved the polymer and releases the mRNA to the aqueous phase. The extracted mRNA were quantified and transfected to the cells using lipofectamine. The results (Supplementary Figure S4G) show that the extracted mRNA was biologically active and translational capacity was equivalent to native untreated mRNA. Finally, the potential toxicity of the nanoparticles was assessed by determining the cell viability after incubation with the nanoparticles for 72 hours compared with untreated cells (Supplementary Figure S5). No toxicity was observed up to the highest concentration of 1000 µg/ml.

Endosomal escape of PLA-lipid composite NPs

The PLA-PEG i-NPs with encapsulated intact and biologically active mRNA were tested on the A549-CD7 cells for their ability to deliver mRNA to the cytosol for translation by endogenous ribosomal machinery. Fluorescent particles with encapsulated EYFP mRNA (with or without conjugated anti-CD7 antibody) were incubated with A549-CD7 and viewed by confocal microscopy. This showed i-NPs were efficiently internalised by the cells (Supplementary Figure S6A) but there was no evidence of EYFP mRNA translation into fluorescent protein. Further, flow

cytometry analysis confirmed there was little EYFP protein translation from mRNA, even with the i-NPs (Supplementary Figure S6B, C). It appears that the NPs are engulfed by endocytosis but they become trapped inside these vesicular structures and fail to release their content to the cytosol.

Cationic polymers and lipids are known to exhibit endosomolysis by proton sponge effect [52, 53] and to facilitate this, DOTAP was includes in the NPs, since DOTAP is a cationic lipid widely used for the cytosolic delivery of nucleic acids [54-56]. Lipid polymer composite nanoparticles were therefore prepared by incorporating this endosomolytic lipid in the PLA-PEG polymer at the level of either 5% or 10% of the total polymer content. Confocal microscopy analysis of A549-CD7 cells incubated with NP-DOTAP or i-NP-DOTAP indicated that these cationic lipids facilitated breakage of the vesicular entrapment resulting in homogeneous distribution within the cytosol (Figure 4, Supplementary Figure 7). Co-localisation of the anti-LAMP-1 endo-lysosomal marker was confirmed in anti-CD7 i-NPs (Figure 4C). In addition, the i-NPs with incorporated DOTAP cationic lipid retained the CD7-specific association and uptake and the NPs lacking anti-CD7 did not enter the cells (Figure 4 A, B).

Modified mRNA was encapsulated within NPs that were made with either 5% or 10% DOTAP and with or without conjugated of anti-CD7 antibody and the NPs were labelled with Alexa Fluor 555. These NPs were incubated for 1 to 3 days with A549-CD7 cells. After incubation, cells were recovered and flow cytometry used to assess fluorescence signal from translation of released EYFP mRNA and fluorescence from the particles themselves (Figure 5). The non-antibody conjugated NPs in each case did not yield EYFP fluorescence with DOTAP-modified NPs. However, antibody-conjugated i-NPs-DOTAP displayed small levels of fluorescence resulting from the delivered mRNA and translation with either 5% (Figure 5A) or 10% DOTAP incorporation (Figure 5B). mRNA translation was not altered by varying amounts of mRNA used at 24 hours and was similar whether 5% (Figure 5C) or 10% (5D).

i-NP-DOTAP in spleen cells after *in vivo* administration

In vivo biodistribution studies were carried out in transgenic mice expressing human CD7 in spleen and thymus [57] using 5% DOTAP NPs concentration with encapsulated EYFP modified mRNA. The NPs were labelled with the near infrared fluorescent DiR dye to facilitate visualisation in whole animal tissues using an imager IVIS (Perkin Elmer). Figure 6A shows measurements of the fluorescence intensity of thymus, spleen, lung, liver and kidney collected 24 hours and 48 hours after intravenous administration of the nanoparticles. These fluorescent data are quantitated in Figure 6B. Tissue association was found when anti-CD7 conjugated i-NPs was systemically delivered as we observed staining of the spleen and some in liver. When unconjugated NPs were employed, the predominant fluorescence was observed in the liver of the recipient mice and lower amounts in spleen (some in kidney-associated fluorescence was also seen) as would be expected from lack of targeted tissue association We observed very little staining of the thymus with anti-CD7 conjugated i-NPs, despite their being human CD7-expressing thymus cells.

The biodistribution profiles and deposition of the i-NPs selectively to the spleen was confirmed by confocal microscopy with isolated cells from the tissues. Spleens were fixed after resection, cryosectioned and mounted on slides after staining with DAPI (for nuclear staining). Figure 6C displays high deposition of the i-NPs with spleen cells compared to the NPs. These data show only that the fluorescent i-NPs are associated with spleen cells and not whether the NPs are endocytosed into cells when they have engaged the human CD7 on the surface of the cells and whether these i-NPs release their mRNA cargo for translation into EYFP. Accordingly, EYFP fluorescence was evaluated in single cell suspension of spleen of the treated mice analysed by flow cytometry (Figure 6C). Fluorescence of both NP and i-NP is evident in spleen cells, as expected from the whole organ imaging (Figure 6A), but there is a larger number and higher intensity when the i-NPs

were used. It is, however, unclear if the particles are partly internalized or simply associated with the CD7 surface proteins. When the spleen cells were examined by flow cytometry, the amount of fluorescence resulting from expression of EYFP is only fractionally greater in mice treated with i-NPs compared with non-conjugated NPs (Figure 6D).

Discussion

Recent advances have revealed many intracellular molecular targets for diseases, such as cancer, but many have been considered undruggable because of their intransigence to drug therapy, like the RAS family, or because they are transcription factors that emanate from chromosomal translocation events [58]. By employing biological protein reagents (macrodrugs) such as antibody fragments [59], monobodies [60] or affimers [61], a new landscape of molecules has appeared. The delivery of such macrodrugs is a challenge because of their size and potential antigenic properties if systemically delivered. On the other hand, viral vectors to express macromolecules are in clinical trials but they are associated with potential toxicity and complicated/expensive handling. Non-viral vectors are potential more versatile and are currently, the most abundant in FDA-approved clinical trials [35, 36] especially for short RNA, such as shRNA. Our work offers an alternative to deliver modified mRNA using a lipid modified polymeric nanoparticulate system that can target delivery to a desired cellular site by conjugation of monoclonal antibody to an external surface of the particles. We have used the modified version of mRNA with pseudo-uridine that renders mRNA insensitive to various degradation/digestive cellular pathways giving a longer half-life for translation [25, 49].

Immuno-nanoparticles targeting CD7-expressing cells *in vitro*

In our current work, PLA-PEG polymeric nanoparticles have been developed with anti-CD7 antibodies on their surface. These mono-methylether derivatives of PEGs had one side blocked with a methyl group and the other side had either an hydroxyl group or a maleimide group for the conjugation of antibodies in order that conjugated antibodies become the primary face of the nanoparticles. These functionalised particles were shown to be specifically endocytosed by CD7-positive T-cells and in a lung adenocarcinoma cell (A549) that ectopically expresses human CD7 (A549-CD7). Confocal analysis of the A549-CD7 cells incubated with i-NPs confirmed the

internalization of the nanoparticles via specified receptor mediated endocytosis pathway and NPs could be seen inside the cells as soon as 30 minutes after treatment.

All CD7 positive cells showed good uptake of the nanoparticles whereas there was no observed association with three CD7-negative cell lines, the mouse erythro-leukaemia (MEL), mouse myeloma (NS0) or the human Burkitt's lymphoma cell line (Raji). Two different monoclonal antibodies (anti-GPR56 and anti-CD53) were conjugated to the nanoparticles for confirmation of the antibody dependent uptake of nanoparticles. KOPT-K1 cells that express CD7, CD53 and GPR56, were incubated with the i-NPs followed by flow cytometry and this confirmed that uptake of nanoparticles is antibody-dependent.

Our aim was to evaluate cell-specific endocytosis of our nanoparticles and potential for endosomal release of the mRNA cargo. DOTAP is a cationic lipid for the intracellular gene delivery that helps nanoparticles break the endosomal membrane and release nucleic acids into the cytosol [54, 56]. We have employed DOTAP as a mixture with the poly-lactic acid polymer producing DOTAP-modified polymer lipid composite immuno-NPs. Initial tests of cell viability following treatment of cells with i-NP-DOTAP for 72 hours showed no signs of toxicity, even at high amounts of nanoparticles (Supplementary figure 5). By varying the percentage of DOTAP, we found that the range from 5%-10% was optimal (Figure 5) and that 20% DOTAP did not show any significant improvement (data not shown). The cell uptake of these i-NP-DOTAP with encapsulated, modified mRNA and subsequent release of mRNA and its translation into EYFP was assessed in A549-CD7 cells. This showed that the cells were only able to translate minimal EYFP reporter protein that was similar to the positive control (Lipofectamine™ MessengerMAX complexed mRNA).

Immuno-nanoparticles selectively find CD7-expressing cells *in vivo* after systemic delivery

When nanoparticles are introduced into the blood stream, they are subject to several routes to destruction that must be overcome for their effective use [62]. In the circulation, interaction occurs with blood cells and also with blood vessel endothelium and also phagocytosis of the NPs occurs causing non-specific accumulation is spleen and liver. PEGylated systems are widely used for use in systemic delivery and was the principle behind the first FDA approved nanoparticulate formulation Doxil™ [63]. We therefore selected the PLA-PEG block co-polymer for the formulation of PEGylated nanoparticles since PLA is an FDA-approved biodegradable polymer for internal use in human and has shown efficiency to provide safe homing and controlled release of macromolecules [64].

In order to mitigate the risk of non-specific associations of NPs *in vivo*, a PEGylated corona was used with PEG chain lengths optimized for the repulsive forces of cell membranes and attraction forces for entry of the i-NP-DOTAP into T-cells via CD7-mediated endocytosis. The PEG corona should reduce association with the cells in the absence of any ligand. We evaluated various PEG chain lengths (2000, 3400 and 5000 Da) for efficiency in avoiding non-specific uptake of the nanoparticles by the cells and nanoparticles were optimized for encapsulation of the mRNA along with desired particle size (>200 nm) (Table 1). When anti-CD7 antibody was attached to the nanoparticle surface, only a slight increase in the diameter was observed, due to the steric occupation of the antibodies on the corona. Moreover, PEG repulsive forces did not hinder endocytosis of the nanoparticles into cells after adherence to the CD7 receptors. Whilst PLA-PEG2000 nanoparticles showed some non-specific binding, those prepared with PLA-PEG3400 and PLA-PEG5000 did not.

The biodistribution and mRNA delivery *in vivo* was analysed in humanized transgenic mice that express human CD7 on leucocytes [Schanberg1995]. After the administration of i-NP-DOTAP via the tail vein of these mice, fluorescence imaging of resected organs showed that the nanoparticles accumulate primarily in the spleen and a lesser amount in liver whereas unconjugated NP-DOTAP was mainly

deposited in the liver and relatively little in spleen (Figure 6). These results were further confirmed by the immunohistochemistry where i-NP-DOTAP can be seen in transgenic mouse spleens but relatively little when NP-DOTAP was administered (Figure 6C). The ability of these i-NP-DOTAP to deliver EYFP reporter mRNA to cells *in vivo* was assessed after administration of i-NP-DOTAP-mRNA to the transgenic mice on three consecutive days. After this, the spleens were analysed for potential expression of reporter EYFP protein from delivered mRNA using flow cytometry of isolated spleen cells (Figure 6D) but little expression was evident and essentially no difference with the i-NP-DOTAP or NP-DOTAP. Therefore, our results show that the anti-CD7 conjugated i-NP-DOTAP are preferentially targeted to transgenic mouse splenocytes expressing CD7 but that this nanoparticle system requires significant optimization for *in vivo* delivery of macrodrugs in the form of mRNA into cells via surface antigen mediated endocytosis.

The CD7 antigen receptor shows rapid internalization after binding to the ligand or anti-CD7 antibody that makes a suitable to be used for the receptor mediated endocytosis of the cargo and has been choice of the marker for targeting T-ALL [45, 65]. Our current work combines the ability of the anti-CD7 conjugated DOTAP modified PLA-PEG lipid polymer composite nanoparticles to remain stable in the blood stream after systemic delivery and deliver mRNA for protein translation in cells expressing CD7 antigen *in vivo*. This can equally be applied to other surface markers where the antibody binding causes endocytosis. In the case of CD7, it is expressed on T-cell acute leukaemias [66] and a subset of acute myeloid leukaemias but not on vital organs such as brain, heart, lung and kidney [67]. Thus, the nanoparticle system described here is a valuable tool to develop clinically translatable vector/cargo for delivery of macrodrugs against these cancers.

Materials and Methods

Tissue culture

A549 human lung adenocarcinoma cells and murine erythroleukemia cells (MEL) were grown in DMEM media supplemented with 10% FBS (Sigma); mouse myeloma NS0, T cell line Jurkat, KOPT-K1, the Burkitt's lymphoma line RAJI were grown in RPMI medium (Life Technologies) supplemented with 10% FBS 37°C with 5% CO_2. Cell lines were verified by analysis of *RAS* mutation isoform genotypes and, in the case, of KOPT-K1 by the presence of the t(11;14) translocation [68].

A549-CD7 cell line generation

A549-CD7 cells were generated by stable transfection of pCDNA3.1-Zeo$^+$-CD7 into A549 cells. pCDNA3.1-Zeo$^+$-CD7 was linearized at BglII site and transfected with polyethlylamine (PEI, Sigma Aldrich) condensation into A549. After 48 hours, cells were serially diluted to obtain single cell suspensions and clones were grown in the presence of 500µg/mL Zeocine™ (ThermoFisher Scientific). After four weeks, cell colonies were picked and were evaluated for CD7 expression by flow cytometry (Attune NxT Flowcytometer, ThermoFisher Scientific) after staining with PE-anti-CD7 antibody (BD Biosciences). One clone was selected based on CD7 protein expression using a FACSAriaII (BD Biosciences) and cells were maintained in DMEM, 10% FBS containing 100µg/mL Zeocine. This clone is called A549-CD7 herein.

mRNA synthesis

Pseudo-uridine modified mRNA encoding EYFP was synthesized using an *in vitro* transcription kit (MEGAScript® T7 transcript kit, Thermo Fisher Scientific, AM1333). The template plasmid was constructed by cloning EYFP gene, amplified by PCR from pEYFP-N1 vector, into pTnT™ vector (Promega, L5620) between EcoRI and NotI restriction sites to produce pTnT-EYFP-N1 plasmid. This template plasmid was linearised by BamHI digestion, followed by a 30 min treatment with 0.5% SDS and 0.1mg/mL Proteinase K at 50˚C, and finally purified by QIAquick PCR purification kit

(Qiagen, 28104). *In vitro* transcription reaction was set up according to the manufacturer's instructions. Uridine was substituted with pseudo-uridine (Insight Biotechnology) and guanidine was partially substituted with ARCA cap (New England biolabs) to obtain a molar ratio of 1:4 (1.5mM:6mM with a final concentration of 7.5mM equal to other NTPs). The transcription reaction was incubated for 4 hours at 37˚C followed by treatment with TRUBO DNAase for 15 minutes at 37˚C. Synthesized mRNA was purified by MEGAClear™ Transcription Clean-up Kit (Thermo Fisher Scientific, AM1908) by the manufacturer's instructions, quantified by UV spectroscopy (Nanodrop ND-8000) and verified by electrophoresis on 2% agarose gels. Biological activity was assessed by transfecting the purified mRNA into Jurkat or A549-CD7 cells after complexing with Lipofectamine™ MessengerMAX reagent according to manufacturer's instructions. The protein product was detected by fluorescence microscopy with the EYFP filter after 16 hours. The level of expression of the EYFP which was quantified by the flow cytometry (Attune NxT Flowcytometer, ThermoFisher Scientific).

Synthesis of antibodies and characterization

A stable NS0 myeloma cell line producing recombinant anti-CD7 antibodies (IgG1) was established (JZ and THR, unpublished). Cells were grown in RPMI media supplemented with 10% FCS, 1x Penicillin-Streptomycin (100 units/mL Penicillin and 100µg/mL Streptomycin), 0.2 mg/mL G418 (Geneticin, Selection antibiotic, Sigma Aldrich) in a roller bottle gassed with 5% CO_2 and incubated at 37˚C. After 7 days, the cell were removed by centrifugation and the supernatant filtered through a 0.2µm filter. Antibodies were purified with Protein G column chromatography (HiTrap Protein G HP antibody purification columns, GE Healthcare, Life Sciences) using an Äkta Start (GE Healthcare, Life Sciences). Supernatants were passed through the column at 1mL/min to bind antibodies in the presence of 20mM Sodium Phosphate, pH 7.0. The column was washed with 10CV of 20mM Sodium Phosphate buffer and eluted with 0.1M Glycine (pH 2.7) directly into Tris buffer pH 8.9. The buffer was

exchanged into 1x PBS by repetitive centrifugation with Amicon ultra centrifugal filters (MWCO 10kDa, Millipore) and concentrated to 1 mg/ml. Antibody batches were validated by titrating against CD7 expressing cells using FITC-IgG secondary antibody by flow cytometry with a unit number of cells and serial dilution on ice for an hour, washed and incubated with secondary antibody with FITC for 30 minutes. Cell samples for flow cytometry were prepared by washing and re-suspension in 5%FCS in PBS and analysed compared to cells treated with secondary antibody only.

Synthesis of PLA-PEG

MAL-PEG3400-OH or MAL-PEG2000-OH (340 mg) (from JenKemUSA) was dissolved in toluene (12 mL) before addition of D,L-lactide (1.87 g, 13.0 mmol), followed by Sn(Oct)2 (23 mg, 5.7 µmol). The resultant corresponding solutions were heated to reflux for 16 h, cooled down and concentrated *in vacuo (*using of a rotary evaporator attached to a diaphragm pump). The obtained white oils were dissolved in dichloromethane/methanol (10:1, 5 mL) and precipitated using diethyl ether cooled to -78 °C. The solids were filtered rapidly to minimize warming and dried *in vacuo* to obtain the desired polymer as a white solid. The resultant PLA-PEG compounds were confirmed by proton NMR spectra recorded on Bruker Avance spectrometers (AVII400 or AVIII 400) in the deuterated solvent stated. The field was locked by external referencing to the relevant deuteron resonance. ^{1}H NMR (400 MHz, $CDCl_3$) δ = 5.19-5.15 (m, $OCCH(CH_3)O$- in PLA), 3.65 (s, $-CH_2CH_2O$- in PEG), 1.59-1.55 (m, $-OCCHCH_3O$- in PLA); for pla-peg2k, r = 0.27; for pla-peg3.4k, r = 0.51.

Formulation and characterization of nanoparticles

Nanoparticles were prepared by a double emulsion solvent evaporation method. An internal aqueous phase, composed of mRNA and 0.1% BSA, was added drop-wise whilst vortexing, to an organic phase, comprised of 4% w/v poly-lactic acid polymer in dichloromethane. An emulsion was obtained by subjecting this mixture to probe sonication at 50% amplitude for 20 seconds pulsatile sonication (10 sec cycles with 3 sec pause) on a Branson digital sonifier (equipped with 3mm microtip). This primary

water/oil emulsion was added to an external aqueous phase (5% polyvinyl alcohol solution, 87-90% hydrolysed 30-70 kDa, Sigma) dropwise under continuous vortexing and probe sonicated again for 40 seconds. This secondary water/oil/water emulsion was diluted with 2x volume of MilliQ water and stirred for 3 hours to evaporate the organic solvent. The nanoparticles were collected by centrifugation at 40,000g for 20 mins (Avanti J-30, Beckman Coulter centrifuge). Pellets were washed twice to remove free polyvinyl alcohol and NP yield was determined by drying a unit amount of NP suspension in a hi-speed rotary evaporator, which was used for dose calculations in the experiments. The same method was used for the preparation of nanoparticles with all the polymers; PLA-PEG2000, PELA-PEG3400 and PLE-PEG5000. To prepare polymer lipid composite nanoparticles with DOTAP, 5% or 10%w/w polymer was replaced with DOTAP lipid maintaining the total lipid polymer content at 4% w/v in the organic dichloromethane phase.

To prepare fluorescent NPs, PLA-AlexaFlour 555 polymer was synthesized using EDC/NHS chemistry. The PLA-AlexaFlour 555 polymer was added to 2.5% w/w of total polymer weight in the organic phase during the nanoparticle preparation. 0.01 mmole PLA and 0.1 mmole 1-Ethyl-3-(3-dimethylaminopropyl) carbodiimide (EDC) in dichloromethane were mixed together and stirred for 10 min. In parallel, 0.1 mmole N-hydroxysuccinimide (NHS) was dissolved in DMSO before diluting in dichloromethane to give 100mM solution and mixed with the polymer solution. This solution was stirred overnight and the resultant activated PLA was precipitated using an ice-cold mixture of methanol and diethyl ether (10x volume of polymer solution). This activated PLA was mixed with AlexaFlour555 dye in 3:1 molar ratio in dichloromethane and vortexed overnight after addition of diisopropylethylamine (DIPEA) (10x moles of polymer). Finally, dye conjugated polymer was precipitated with ice-cold methanol:diethyl ether mixture and this step was repeated to ensure removal of free unconjugated dye from the polymer.

Conjugation of immuno-NPs

For the preparation of antibody-coated immuno-nanoparticles, the antibodies were thiolated with Traut's reagent (2-iminothiolane) to convert their primary amine groups to thiol groups for reaction with maleimide groups available on the surface of NPs at terminal end of their PEG corona for conjugation. Antibodies were treated for 2 hours with 2-iminothiolane at a 1:40 molar ratio in PBS pH 7.4 (typically 200µg protein in 500µl). Nanoparticles were added to these thiolated antibodies to obtain a ratio of 20µg antibody per mg of nanoparticles and were further incubated for an hour at room temperature to allow thiol-maleimide conjugation. Finally, nanoparticles were collected and washed to remove unconjugated antibody by centrifugation at 16000g for 60 mins.

For *in vivo* studies, nanoparticles were labeled with a near IR fluorescent dye, lipophilic carbocyanine DiR. 1% w/w DiR dye to the total polymer weight was added to the organic phase during nanoparticle preparation. The formulations were prepared in aseptic conditions and were finally filter sterilized by passing through 0.2 µm filters before use in animals.

Nanoparticle tolerability and mRNA expression *in vitro*

A549-CD7 cells (2000 cells per well) were seeded in black 96-well microplates (PerkinElmer) and cultured at 37 °C in 5% CO_2 atmosphere overnight. Different dilutions of the NPs, in the range of 0 to 1000 µg/mL, were added and the cells incubated for 72 hours. Cell viablity was determined using PrestoBlue according the manufacturer's protocol and fluorescence signals measured with an Envision 2103 Multilabel Microplate Reader (PerkinElmer). The fluorescence signals obtained from the nanoparticles treated cells (normalized against medium-only wells) are presented as the percent of the signal for untreated cells, considered to be 100% viable.

Nanoparticle uptake into adherent cells (A459 and A549-CD7) and non-adherent mouse cells was determined differently. For adherent cells, 100,000 cells were seeded in each well of a 24-well plate the day before treatment. Unit amounts of

nanoparticles were added to the wells (final culture volume was 500µl) and incubated at 37˚C and the time of incubation was dependent on the experiment. After treatment, cells were recovered by adding 50µl of 0.5%w/v trypsin to each well and incubated for 5 minutes at 37˚C. 500µl of DMEM media with 10% FCS was added for neutralization of trypsin and cells were harvested by centrifuging at 2000g for 5 minutes. The cell pellets were gently re-suspended in 200µl cold 5% FCS in PBS with DAPI (1µg/mL) and held on ice until analysed by flow cytometry (Attune NxT Flowcytometer, ThermoFisher Scientific). For mRNA expression studies, 50,000 cells were seeded in the each well and the same procedure was used.

For non-adherent (suspension) cells, 200,000 cells were seeded in a non-tissue culture treated 24-well plate 2 hours prior to incubation. Unit amounts of nanoparticles were added to the wells and incubated at 37˚C for the duration of study. Cells were harvested by pipetting, centrifuged at 2000g for 5 min and re-suspended in 500µl cold 5%FCS in PBS for analysis by flow cytometry.

For confocal microscopy, cells were seeded on 8-chambered glass slides (Nunc Lab-Tek II, Thermo Fisher Scientific). After being treated with NPs, cells were washed with cold PBS and fixed with 4% PFA in PBS for 5 min at RT. Nuclei were stained with DAPI (1mg/mL) for two minutes, washed twice with cold PBS and were mounted with non-curing SlowFade™ Diamond Antifade Mountant (Thermo Scientific). For anti-LAMP-1 staining after fixing cells were permeabilised by incubating with 0.5% Tween20 in PBS (PBST) for 15 min at room temperature, blocked with 10% FBS in PBST to avoid non-specific antibody binding. The slides were washed twice with PBST and incubated with AlexaFlour647-anti-human LAMP1 antibody (Biolegend) at room temperature for 1 hour to detect late endo-lysosomes. Excess antibody was removed by washing twice with PBST and stained with DAPI for nucleus, washed again twice with cold PBS and were mounted with non-curing SlowFade™ Diamond Antifade Mountant (Thermo Scientific). Samples were analyzed using a Zeiss 880 Inverted Confocal Microscope.

572 ***In vivo* tolerance, biodistribution and *in vivo* mRNA expression studies**

573 For *in vivo* biodistribution studies transgenic mice expressing huCD7 mice were
574 employed [57]. The donor NP formulations were labeled with near IR fluorescent dye
575 DiR (as described above), prepared aseptically and were injected via tail vain (200µg
576 of NPs in 100µL PBS). All the mice were closely monitored up to 120min post-
577 injection for possible adverse effects (such as hunched gait, pilorection, inertia,
578 breathing problems) and thereafter regularly until the humane end point. The mouse
579 work was carried out as Regulated Procedures under a Home Office Approved
580 license. None of the mice showed any abnormal features during the course of any of
581 the studies. For biodistribution study mice were sacrificed 6, 24 and 48 hours after
582 NP administration and were dissected to harvest vital organs. After washing in ice-
583 cold PBS, the resected organs were arranged over a imaging sheet and were taken
584 into the imaging chamber of an IVIS imager (Lumina LT, Perkin Elmer).
585 For the localization of the NPs in the spleen cells, confocal analysis was performed.
586 After IVIS imaging, the spleens were fixed in neutralized buffered 10% formalin at
587 4˚C for 1 hour, washed twice with cold PBS and submerged in 20% sucrose solution
588 at 4˚C. Tissues were washed and transferred to cryo-preservative OCT-filled molds
589 and snap frozen at -80˚C. These molds were cut into 10µm sections using a cryostat
590 operating at -20˚C operating. Sections were stained with DAPI (1µg/mL) for nuclei,
591 washed twice and mounted with SlowFade™ Diamond Antifade Mountant (Thermo
592 S36963) for confocal analysis. Confocal analysis was performed on a Ziess LSM880.
593 For *in vivo* mRNA expression of mRNA released from nanoparticles, i-NPs were
594 loaded with mRNA coding for reporter gene EYFP and these nanoparticles were also
595 tagged with DiR dye to locate the nanoparticles after the administration in the mice
596 and to monitor clearance from the body. Tg-hCD7 mice received 3 intravenous
597 injections of the nanoparticles on 3 consecutive days and were checked for any
598 adverse reaction at regular intervals. After 48 hours from the last injection, mice were
599 sacrificed and spleens were collected and immediately place on ice in cold PBS

containing 5% FCS. For flow cytometry, single cell suspensions were prepared by mashing the spleen tissue using a 2 ml syringe plunger and making the single cell suspensions by passing through a 70 µm cell strainer. Ice cold PBS with 5% FCS was used to wash and cells were harvested by centrifugation. Single cells suspensions were treated with red blood cell lysis buffer for 2-4 minutes before fixing them with 4% PFA at room temperature for 15 minutes prior to flow cytometry analysis.

608

609 **Resource List**

	Name	Source	Catalogue Number
Plasmid	EYFP-N1	BD Biosciences	6006-1
Plasmid	pTnT	Promega	L5610
Plasmid	pCDNA3.1-Zeo^{+}-CD7	Gifted by Prof. Linda Baum	NA
Antibody	FITC-IgG	Invitrogen	62-8411
Antibody	Alexa Fluor647 antiHuman CD107a (LAMP-1)	Biolegend	328612
Antibody	PE Mouse Anti-Human CD7	BD	555361

610

611

Acknowledgements

This work was supported by grants from Bloodwise (12051) and the Medical Research Council (MR/J000612/1). We would like to thank Prof. Bart Haynes (Duke University) for generously providing the humanized CD7 transgenic mouse strain and Prof. Linda Baum for the pcDNA3.1-ZEO cD7 human CD7 expression vector.

Conflict of interest statement

The authors have no conflicts of interest to declare.

Author's contributions

Participated in project & research design: AJ, THR

Conducted experiments: AJ, CB, JZ, SM, AM

Performed data analysis: AJ, JZ, THR

Wrote or contributed to the writing of the manuscript: all authors

Additional information: Supplementary Information accompanies this paper

References

1. Druker BJ, Talpaz M, Resta DJ, Peng B, Buchdunger E, Ford JM, Lydon NB, Kantarjian H, Capdeville R, Ohno-Jones S, Efficacy and safety of a specific inhibitor of the BCR-ABL tyrosine kinase in chronic myeloid leukemia. New England Journal of Medicine, 2001;344(14):1031-1037.
2. Rossari F, Minutolo F, Orciuolo E, Past, present, and future of Bcr-Abl inhibitors: from chemical development to clinical efficacy. Journal of hematology & oncology, 2018;11(1):84.
3. Griffin M, Scotto D, Josephs DH, Mele S, Crescioli S, Bax HJ, Pellizzari G, Wynne MD, Nakamura M, Hoffmann RM, BRAF inhibitors: resistance and the promise of combination treatments for melanoma. Oncotarget, 2017;8(44):78174.
4. Long GV, Stroyakovskiy D, Gogas H, Levchenko E, de Braud F, Larkin J, Garbe C, Jouary T, Hauschild A, Grob J-J, Chiarion-Sileni V, Lebbe C, Mandalà M, Millward M, Arance A, Bondarenko I, Haanen JBAG, Hansson J, Utikal J, Ferraresi V, Kovalenko N, Mohr P, Probachai V, Schadendorf D, Nathan P, Robert C, Ribas A, DeMarini DJ, Irani JG, Swann S, et al., Dabrafenib and trametinib versus dabrafenib and placebo for Val600 BRAF-mutant melanoma: a multicentre, double-blind, phase 3 randomised controlled trial. The Lancet, 2015;386(9992):444-451.
5. Nam C, Lobato M, Appert A, Drynan L, Tanaka T, Rabbitts T, An antibody inhibitor of the LMO2-protein complex blocks its normal and tumorigenic functions. Oncogene, 2008;27(36):4962.
6. Tanaka T, Williams RL, Rabbitts TH, Tumour prevention by a single antibody domain targeting the interaction of signal transduction proteins with RAS. The EMBO journal, 2007;26(13):3250-3259.
7. Seigneuric R, Gobbo J, Colas P, Garrido C, Targeting cancer with peptide aptamers. Oncotarget, 2011;2(7):557.

8. Reverdatto S, Burz DS, Shekhtman A, Peptide aptamers: development and applications. Current topics in medicinal chemistry, 2015;15(12):1082.

9. Hirayama M, Nishimura Y, The present status and future prospects of peptide-based cancer vaccines. International immunology, 2016;28(7):319-328.

10. Tanaka T, Rabbitts TH, Interfering with protein-protein interactions: potential for cancer therapy. Cell cycle, 2008;7(11):1569-1574.

11. Pérez-Martínez D, Tanaka T, Rabbitts TH, Intracellular antibodies and cancer: new technologies offer therapeutic opportunities. Bioessays, 2010;32(7):589-598.

12. Tanaka T, Rabbitts T, Interfering with RAS–effector protein interactions prevent RAS-dependent tumour initiation and causes stop–start control of cancer growth. Oncogene, 2010;29(45):6064.

13. Tanaka T, Sewell H, Waters S, Phillips SE, Rabbitts TH, Single domain intracellular antibodies from diverse libraries emphasizing dual functions of LMO2 protein interactions using a single VH domain. Journal of Biological Chemistry, 2011;286(5):3707-3716.

14. Noguchi H, Kaneto H, Weir GC, Bonner-Weir S, PDX-1 protein containing its own antennapedia-like protein transduction domain can transduce pancreatic duct and islet cells. Diabetes, 2003;52(7):1732-1737.

15. Console S, Marty C, García-Echeverría C, Schwendener R, Ballmer-Hofer K, Antennapedia and HIV transactivator of transcription (TAT)“protein transduction domains” promote endocytosis of high molecular weight cargo upon binding to cell surface glycosaminoglycans. Journal of Biological Chemistry, 2003;278(37):35109-35114.

16. Do Kwon Y, Oh SK, Kim HS, Ku S-Y, Kim SH, Choi YM, Moon SY, Cellular manipulation of human embryonic stem cells by TAT-PDX1 protein transduction. Molecular therapy, 2005;12(1):28-32.

17. Mintzer MA, Simanek EE, Nonviral Vectors for Gene Delivery. Chemical Reviews, 2009;109(2):259-302.
18. Wilson JM, Adenoviruses as Gene-Delivery Vehicles. New England Journal of Medicine, 1996;334(18):1185-1187.
19. Davis ME, Non-viral gene delivery systems. Current Opinion in Biotechnology, 2002;13(2):128-131.
20. Zufferey R, Nagy D, Mandel RJ, Naldini L, Trono D, Multiply attenuated lentiviral vector achieves efficient gene delivery in vivo. Nature Biotechnology, 1997;15(9):871-875.
21. McIvor RS, Therapeutic delivery of mRNA: the medium is the message. Molecular Therapy, 2011;19(5):822-823.
22. Hajj KA, Whitehead KA, Tools for translation: non-viral materials for therapeutic mRNA delivery. Nature Reviews Materials, 2017;2(17056.
23. Tavernier G, Andries O, Demeester J, Sanders NN, De Smedt SC, Rejman J, mRNA as gene therapeutic: How to control protein expression. Journal of Controlled Release, 2011;150(3):238-247.
24. Kormann MSD, Hasenpusch G, Aneja MK, Nica G, Flemmer AW, Herber-Jonat S, Huppmann M, Mays LE, Illenyi M, Schams A, Griese M, Bittmann I, Handgretinger R, Hartl D, Rosenecker J, Rudolph C, Expression of therapeutic proteins after delivery of chemically modified mRNA in mice. Nature Biotechnology, 2011;29(154.
25. Anderson BR, Muramatsu H, Jha BK, Silverman RH, Weissman D, Karikó K, Nucleoside modifications in RNA limit activation of 2′-5′-oligoadenylate synthetase and increase resistance to cleavage by RNase L. Nucleic acids research, 2011;39(21):9329-9338.
26. Zangi L, Lui KO, Von Gise A, Ma Q, Ebina W, Ptaszek LM, Später D, Xu H, Tabebordbar M, Gorbatov R, Modified mRNA directs the fate of heart

progenitor cells and induces vascular regeneration after myocardial infarction. Nature biotechnology, 2013;31(10):898.

27. Lv H, Zhang S, Wang B, Cui S, Yan J, Toxicity of cationic lipids and cationic polymers in gene delivery. Journal of Controlled Release, 2006;114(1):100-109.

28. Pack DW, Hoffman AS, Pun S, Stayton PS, Design and development of polymers for gene delivery. Nature Reviews Drug Discovery, 2005;4(7):581-593.

29. Stewart MP, Sharei A, Ding X, Sahay G, Langer R, Jensen KF, In vitro and ex vivo strategies for intracellular delivery. Nature, 2016;538(183.

30. Pun SH, Hoffman AS, B.8 - Nucleic Acid Delivery, in Biomaterials Science (Third Edition), B.D. Ratner, et al., Editors. 2013, Academic Press. p. 1047-1054.

31. Anselmo AC, Mitragotri S, Nanoparticles in the clinic: An update. Bioengineering & Translational Medicine, 2019e10143.

32. Shi J, Xiao Z, Votruba AR, Vilos C, Farokhzad OC, Differentially charged hollow core/shell lipid–polymer–lipid hybrid nanoparticles for small interfering RNA delivery. Angewandte Chemie International Edition, 2011;50(31):7027-7031.

33. Yang X-Z, Dou S, Sun T-M, Mao C-Q, Wang H-X, Wang J, Systemic delivery of siRNA with cationic lipid assisted PEG-PLA nanoparticles for cancer therapy. Journal of controlled release, 2011;156(2):203-211.

34. Babu A, Muralidharan R, Amreddy N, Mehta M, Munshi A, Ramesh R, Nanoparticles for siRNA-based gene silencing in tumor therapy. IEEE transactions on nanobioscience, 2016;15(8):849-863.

35. Chakraborty C, Sharma AR, Sharma G, Doss CGP, Lee S-S, Therapeutic miRNA and siRNA: moving from bench to clinic as next generation medicine. Molecular Therapy-Nucleic Acids, 2017;8(132-143.

741 36. Hu B, Weng Y, Xia XH, Liang Xj, Huang Y, Clinical advances of siRNA
742 therapeutics. The journal of gene medicine, 2019e3097.
743 37. Zuckerman JE, Gritli I, Tolcher A, Heidel JD, Lim D, Morgan R, Chmielowski
744 B, Ribas A, Davis ME, Yen Y, Correlating animal and human phase Ia/Ib
745 clinical data with CALAA-01, a targeted, polymer-based nanoparticle
746 containing siRNA. Proceedings of the National Academy of Sciences,
747 2014;111(31):11449-11454.
748 38. Reichmuth AM, Oberli MA, Jaklenec A, Langer R, Blankschtein D, mRNA
749 vaccine delivery using lipid nanoparticles. Therapeutic delivery,
750 2016;7(5):319-334.
751 39. Su X, Fricke J, Kavanagh DG, Irvine DJ, In vitro and in vivo mRNA delivery
752 using lipid-enveloped pH-responsive polymer nanoparticles. Molecular
753 pharmaceutics, 2011;8(3):774-787.
754 40. Zhang J, Shrivastava S, Cleveland RO, Rabbitts TH, Lipid-mRNA
755 nanoparticle designed to enhance intracellular delivery mediated by shock
756 waves. ACS applied materials & interfaces, 2019;11(11):10481-10491.
757 41. Farokhzad OC, Jon S, Khademhosseini A, Tran T-NT, LaVan DA, Langer R,
758 Nanoparticle-aptamer bioconjugates: a new approach for targeting prostate
759 cancer cells. Cancer research, 2004;64(21):7668-7672.
760 42. Hu Q, Gao X, Gu G, Kang T, Tu Y, Liu Z, Song Q, Yao L, Pang Z, Jiang X,
761 Glioma therapy using tumor homing and penetrating peptide-functionalized
762 PEG–PLA nanoparticles loaded with paclitaxel. Biomaterials,
763 2013;34(22):5640-5650.
764 43. Richards DA, Maruani A, Chudasama V, Antibody fragments as nanoparticle
765 targeting ligands: a step in the right direction. Chemical science,
766 2017;8(1):63-77.
767 44. Shargh VH, Hondermarck H, Liang M, Antibody-targeted biodegradable
768 nanoparticles for cancer therapy. Nanomedicine, 2016;11(1):63-79.

769 45. Peipp M, Küpers H, Saul D, Schlierf B, Greil J, Zunino SJ, Gramatzki M, Fey
770 GH, A recombinant CD7-specific single-chain immunotoxin is a potent
771 inducer of apoptosis in acute leukemic T cells. Cancer research,
772 2002;62(10):2848-2855.
773 46. Heald C, Stolnik S, Kujawinski K, De Matteis C, Garnett M, Illum L, Davis S,
774 Purkiss S, Barlow R, Gellert P, Poly (lactic acid)− poly (ethylene oxide)(PLA−
775 PEG) nanoparticles: NMR studies of the central solidlike PLA core and the
776 liquid PEG corona. Langmuir, 2002;18(9):3669-3675.
777 47. Gref R, Lück M, Quellec P, Marchand M, Dellacherie E, Harnisch S, Blunk T,
778 Müller R, 'Stealth'corona-core nanoparticles surface modified by polyethylene
779 glycol (PEG): influences of the corona (PEG chain length and surface
780 density) and of the core composition on phagocytic uptake and plasma
781 protein adsorption. Colloids and Surfaces B: Biointerfaces, 2000;18(3-4):301-
782 313.
783 48. Perry JL, Reuter KG, Kai MP, Herlihy KP, Jones SW, Luft JC, Napier M, Bear
784 JE, DeSimone JM, PEGylated PRINT nanoparticles: the impact of PEG
785 density on protein binding, macrophage association, biodistribution, and
786 pharmacokinetics. Nano letters, 2012;12(10):5304-5310.
787 49. Hornung V, Ellegast J, Kim S, Brzózka K, Jung A, Kato H, Poeck H, Akira S,
788 Conzelmann K-K, Schlee M, 5'-Triphosphate RNA is the ligand for RIG-I.
789 Science, 2006;314(5801):994-997.
790 50. Karikó K, Buckstein M, Ni H, Weissman D, Suppression of RNA recognition
791 by Toll-like receptors: the impact of nucleoside modification and the
792 evolutionary origin of RNA. Immunity, 2005;23(2):165-175.
793 51. Nallagatla SR, Bevilacqua PC, Nucleoside modifications modulate activation
794 of the protein kinase PKR in an RNA structure-specific manner. Rna,
795 2008;14(6):1201-1213.

52. Boussif O, Lezoualc'h F, Zanta MA, Mergny MD, Scherman D, Demeneix B, Behr J-P, A versatile vector for gene and oligonucleotide transfer into cells in culture and in vivo: polyethylenimine. Proceedings of the National Academy of Sciences, 1995;92(16):7297-7301.

53. El-Sayed A, Futaki S, Harashima H, Delivery of macromolecules using arginine-rich cell-penetrating peptides: ways to overcome endosomal entrapment. The AAPS journal, 2009;11(1):13-22.

54. Regelin AE, Fankhaenel S, Gürtesch L, Prinz C, von Kiedrowski G, Massing U, Biophysical and lipofection studies of DOTAP analogs. Biochimica et Biophysica Acta (BBA)-Biomembranes, 2000;1464(1):151-164.

55. Remaut K, Sanders NN, Fayazpour F, Demeester J, De Smedt SC, Influence of plasmid DNA topology on the transfection properties of DOTAP/DOPE lipoplexes. Journal of controlled release, 2006;115(3):335-343.

56. Simberg D, Weisman S, Talmon Y, Barenholz Y, DOTAP (and other cationic lipids): chemistry, biophysics, and transfection. Critical Reviews™ in Therapeutic Drug Carrier Systems, 2004;21(4).

57. Schanberg LE, Lee DM, Fleenor DE, Ware RE, Patel DD, Haynes BF, Kaufman RE, Characterization of human CD7 transgenic mice. The Journal of Immunology, 1995;155(5):2407-2418.

58. Rabbitts TH, Commonality but diversity in cancer gene fusions. Cell, 2009;137(3):391-395.

59. Zeng J, Zhang J, Tanaka T, Rabbitts TH, Single domain antibody fragments as drug surrogates targeting protein–protein interactions inside cells. Antibodies, 2013;2(2):306-320.

60. Koide A, Koide S, Monobodies, in Protein Engineering Protocols2007, Springer. p. 95-109.

822 61. Tiede C, Bedford R, Heseltine SJ, Smith G, Wijetunga I, Ross R, AlQallaf D,
823 Roberts AP, Balls A, Curd A, Affimer proteins are versatile and renewable
824 affinity reagents. Elife, 2017;6(e24903.
825 62. Blanco E, Shen H, Ferrari M, Principles of nanoparticle design for overcoming
826 biological barriers to drug delivery. Nature biotechnology, 2015;33(9):941.
827 63. Barenholz Y, Doxil® — The first FDA-approved nano-drug: Lessons learned.
828 Journal of Controlled Release, 2012;160(2):117-134.
829 64. Jain AK, Massey A, Yusuf H, McDonald DM, McCarthy HO, Kett VL,
830 Development of polymeric–cationic peptide composite nanoparticles, a
831 nanoparticle-in-nanoparticle system for controlled gene delivery. International
832 journal of nanomedicine, 2015;10(7183.
833 65. Frankel AE, Laver JH, Willingham MC, Burns LJ, Kersey JH, Vallera DA,
834 Therapy of Patients with T-cell Lymphomas and Leukemias Using an Anti-
835 CD7 Monoclonal Antibody-Rich a Chain Immunotoxin. Leukemia &
836 Lymphoma, 1997;26(3-4):287-298.
837 66. Pais H, Ruggero K, Zhang J, Al-Assar O, Bery N, Bhuller R, Weston V,
838 Kearns PR, Mecucci C, Miller A, Surfaceome interrogation using an RNA-seq
839 approach highlights leukemia initiating cell biomarkers in an LMO2 T cell
840 transgenic model. Scientific reports, 2019;9(1):5760.
841 67. Sempowski GD, Lee DM, Kaufman RE, Haynes BF, Structure and function of
842 the CD7 molecule. Critical reviews in immunology, 1999;19(4):331.
843 68. Dong W, Xu Y, Hu Q, Munroe D, Minowada J, Housman D, Minden M,
844 Molecular characterization of a chromosome translocation breakpoint t (11;
845 14)(p13; q11) from the cell line KOPT-K1. Leukemia, 1995;9(11):1812-1817.
846
847

Table 1

Nanoparticles	Size (nm)	PDI	Zeta potential (mV)	mRNA Loading (µg/mg)	
				Theoretical	Experimental
PLA-PEG2000	144±12.1	0.091±0.034	-24.5±1.75	-	-
immuno-PLA-PEG2000	149±11.1	0.134±0.031	-25.8±2.52	-	-
PLA-PEG3400	156±4.11	0.136±0.017	-27.1±1.65	-	-
immuno-PLA-PEG3400	171±6.51	0.169±0.017	-24.9±1.59	-	-
PLA-PEG5000	186±7.55	0.157±0.025	-23.9±3.21	-	-
immuno-PLA-PEG5000	198±5.38	0.167±0.034	-25.4±2.32	-	-
mRNA Loaded PLA-PEG3400 Nanoparticles					
immuno-PLA-PEG	173±11.4	0.177±0.056	-26.6±0.80	2.5	1.32±0.05
immuno-PLA-PEG-DOTAP 5%	158±7.02	0.143±0.040	-20.9±1.96	2.5	1.46±0.08
immuno-PLA-PEG-DOTAP 10%	157±9.14	0.132±0.023	-16.2±0.64	2.5	1.52±0.11

Table 1. Physico-chemical characterisation of the nanoparticles.
Size and zeta potential measurements were made using a Zetasizer NanoZS. Each point was recorded as an average of five measurements for a minimum of 10 runs each, and values are the mean of three independently prepared formulations. For the determination of nucleic acid encapsulation efficiency, fluorescent mRNA were synthesized by *in vitro* transcription using FITC-UTP and mRNA were extracted from nanoparticles using chloroform:water and quantified by fluorescence spectroscopy.
In the table, the nanoparticles are PLA-PEG or PLA-PEG-DOTAP NPs. The immuno-nanoparticles refer to respective nanoparticles conjugated with anti-CD7 monoclonal antibody.

Figure Legends

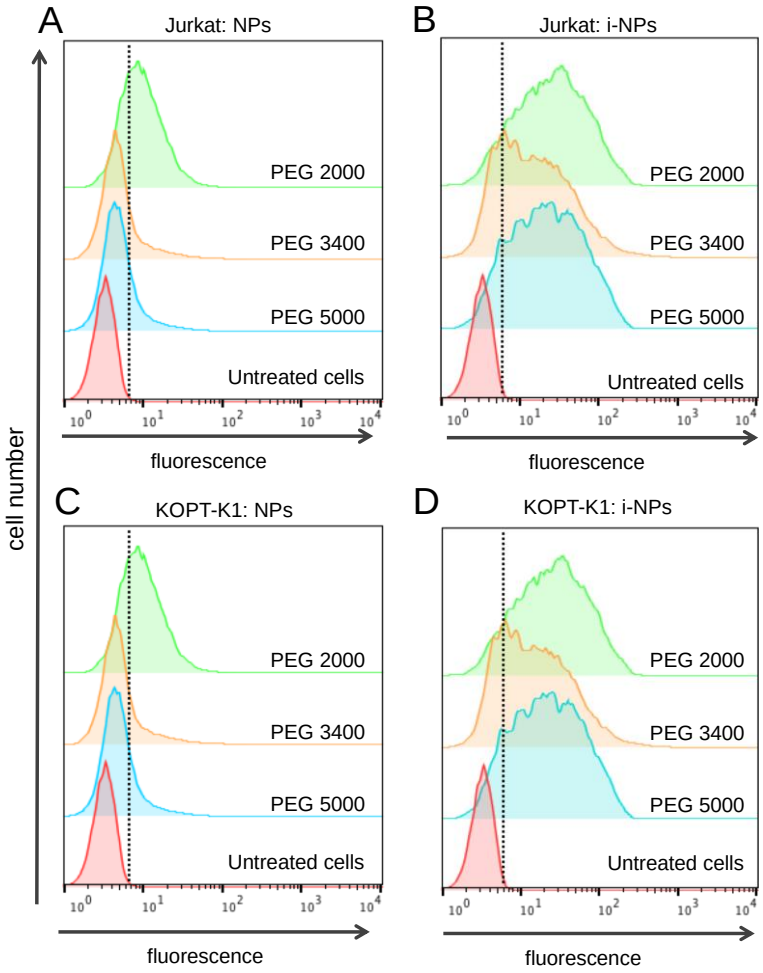

Figure 1. T cell uptake of PLA-PEG nanoparticles with variation of PEG molecular weight

The length of the PEG corona around the nanoparticles was varied with three different PEG chain lengths; 2000, 3400 and 5000 Da. Nanoparticles prepared with these polymers were transfected into human T cell lines Jurkat (panels A, B) or KOPT-K1 cells (panels C, D), both of which express CD7 on the cell surface. The nanoparticles were prepared with and without conjugated anti-CD7 antibody (respectively designated i-NP or NP) and fluorescence was measured by flow cytometry after 4 hours. PLA-PEG2000 NPs showed some non-specific uptake in both cell lines but PLA-PEG3400 and PLA-PEG5000 uptake by cells was only observed when anti-CD7 antibody was conjugated on the nanoparticle surface.

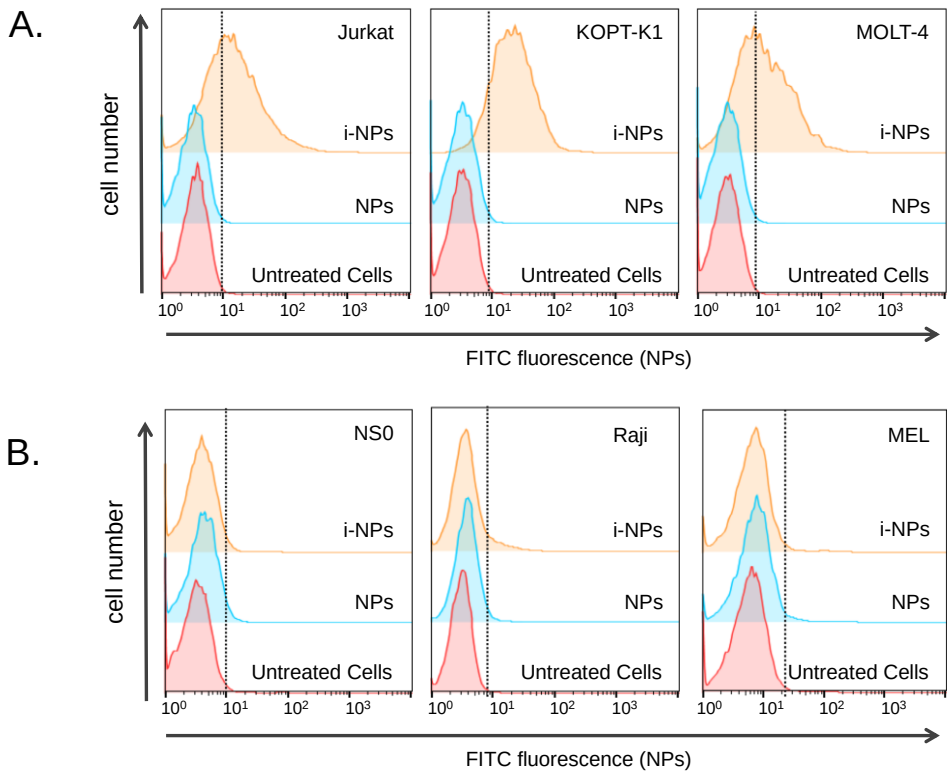

Figure 2. Cell specific uptake of the immuno-NPs by blood cell lines

CD7-expressing T cells Jurkat, KOPT-K1 and MOLT4 (panel A) or CD7-negative mouse myeloma NS0, Burkitt's lymphoma Raji and murine erythro-leukaemia (MEL) (panel B) cells were incubated with PLA-PEG3400 NPs with and without conjugated anti-CD7 antibody (respectively designated i-NP or NP) and labelled with green fluorescence by loading FITC-BSA in the nanoparticles. Fluorescence was determined by flow cytometry after 4 hours of incubation.

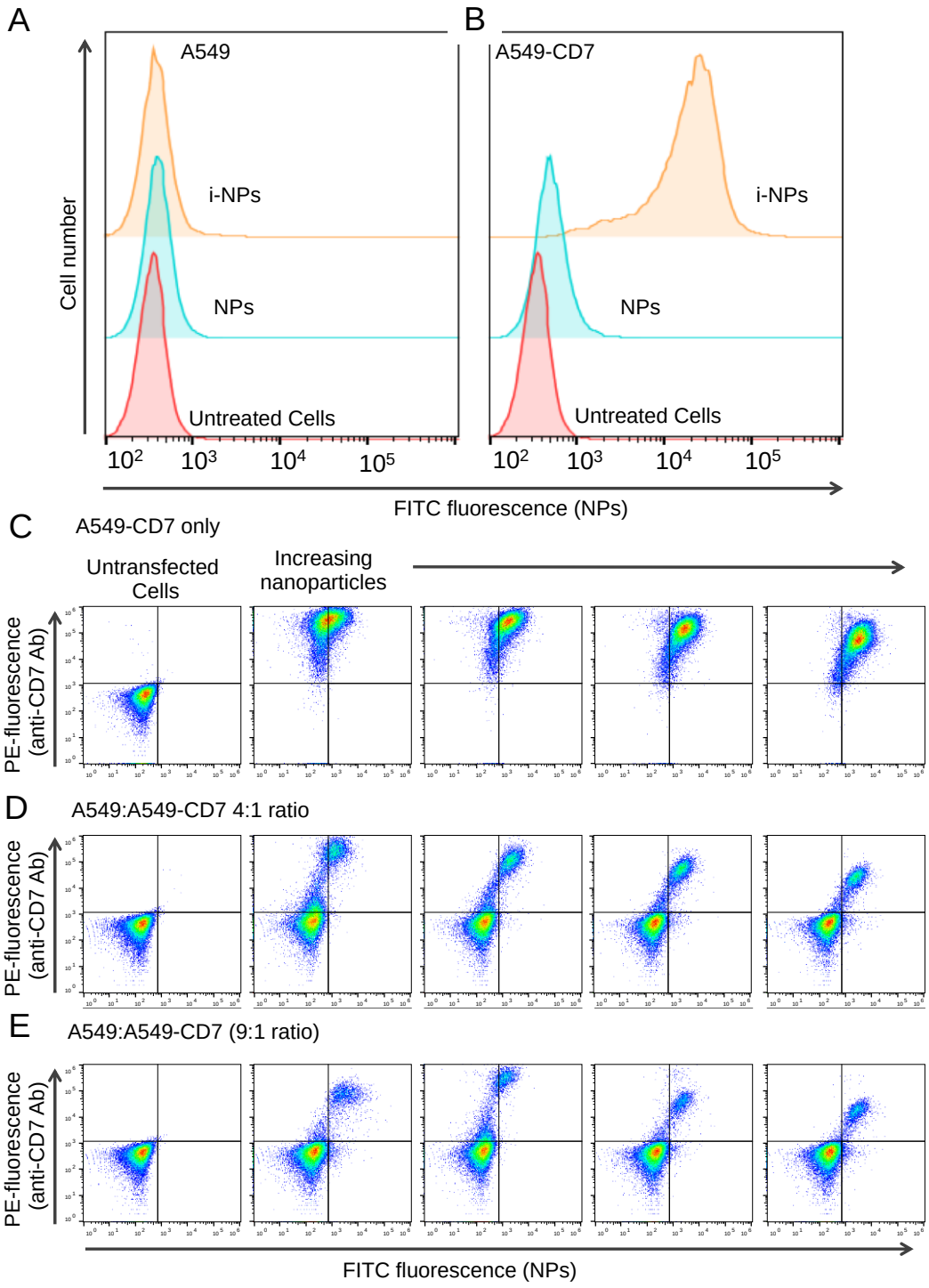

Figure 3. Anti-CD7 immuno-NPs require CD7 surface expression for endocytosis

A549 cells or A549-CD7 cells were incubated with FITC-BSA NPs or FITC-BSA i-NPs for 4 hours and analysed by flow cytometry for assessment of cell uptake. Panel A shows uptake of immuno-PLA-PEG3400 NPs by A549 or, panel B, by A549-CD7, a stable clone expressing human CD7. Uptake was assessed using FITC-NPs and

892 fluorescent (PE) anti-CD7. Fluorescent i-NPs were incubated with A549-CD7 only
893 (panel B), or A549 parental line mixed with A549-CD7 in a ratio of 4:1 (panel C) or
894 9:1 (panel D) for 4 hours and were treated with PE-anti-CD7 antibodies followed by
895 flow cytometry analysis. In panels B-D, the left-hand column shows flow cytometry of
896 control A549 parental cells without nanoparticles while the right hand four columns
897 show flow cytometry of A549/A549-CD7 mixtures following incubation with increasing
898 amount of i-NP (from 10-100 µg per well).
899

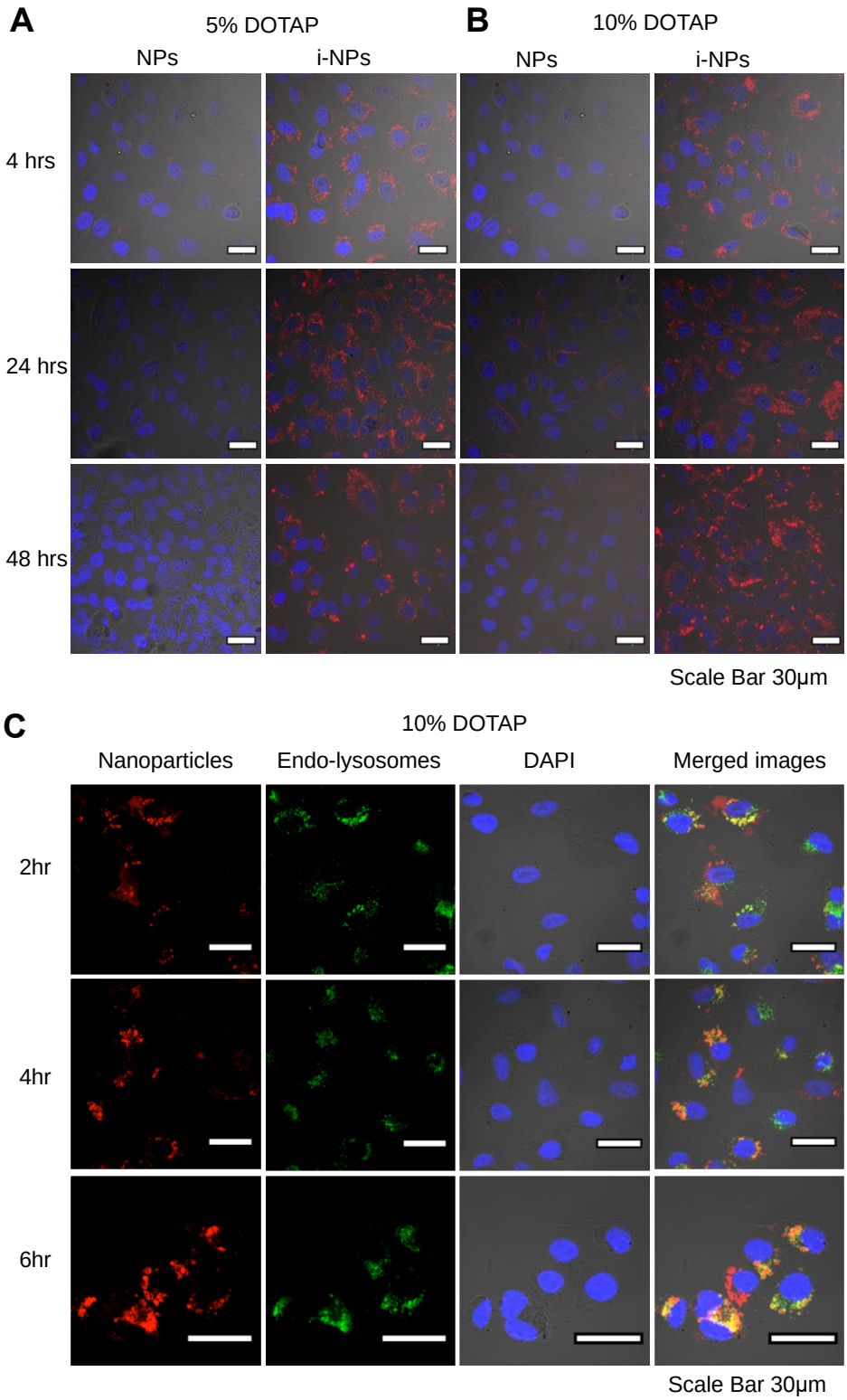

Figure 4. Sub-cellular location of endocytosed i-NPs

A549-CD7 cells were incubated with unconjugated or anti-CD7 conjugated fluorescent nanoparticles (Alexafluor 555, orange staining) for various indicated times and the cells recovered for immuno-fluorescence confocal microscopy, after

staining with DAPI to detect nuclei (blue staining). Panel A shows the uptake of polymer lipid nanoparticles prepared with 5% DOTAP or panel B 10% DOTAP. Panel C shows internalized fluorescent i-NP-DOTAP after different incubation times into A549-CD7 cells that were fixed and cells stained with anti-LAMP-1 antibody as an endo-lysosomal marker. The scale bars represent 20µM. Enlarged images from panel B, 48 hour point of i-NP-DOTAP and from panel C 6 hour merged image are shown in Supplementary Figure S7.

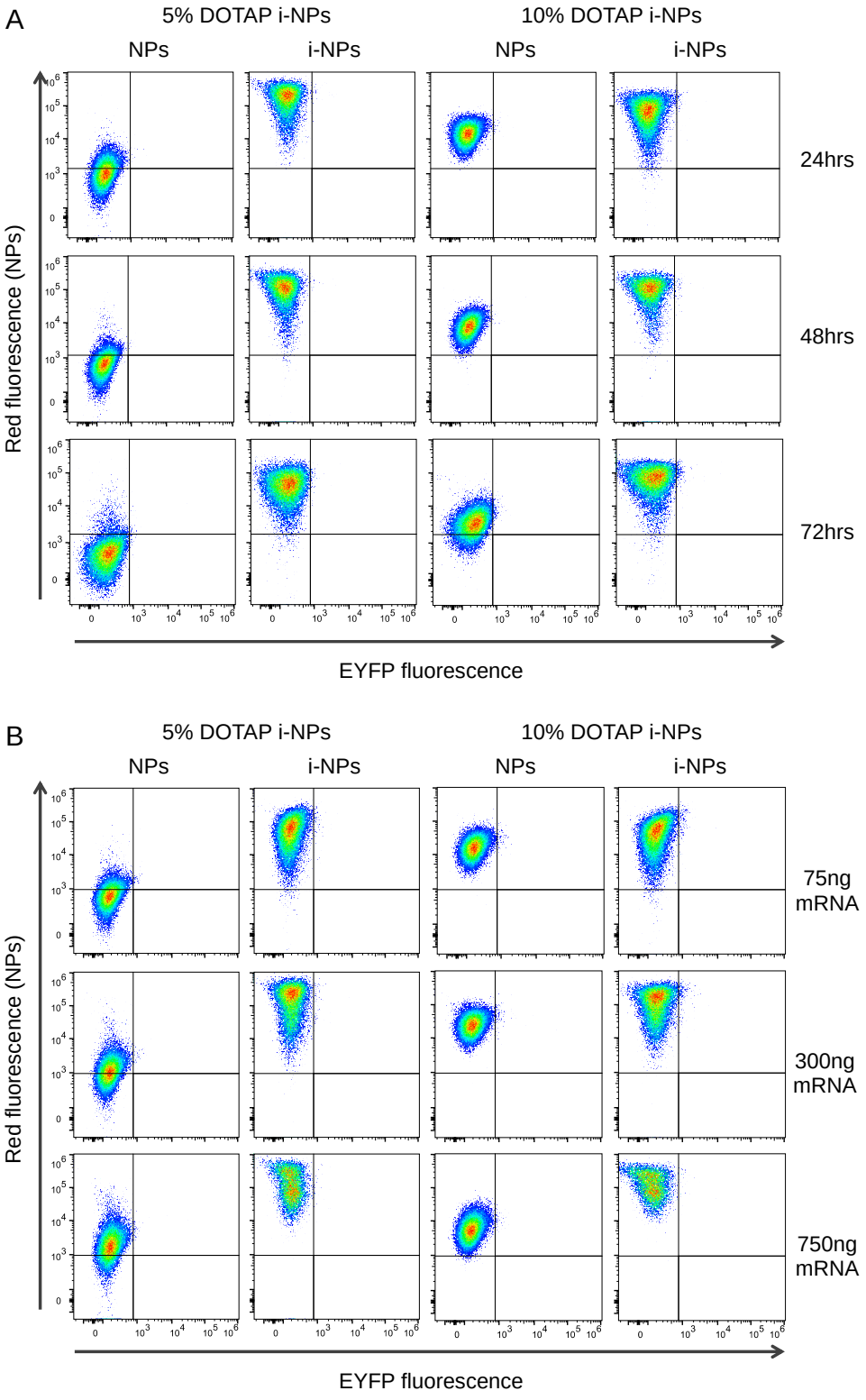

Figure 5. Enhancing PLA-PEG nanoparticle mRNA delivery using DOTAP-modified i-NPs to A549-CD7 cells.

A459-CD7 cells were incubated with Alexa Fluor 555 fluorescent PLA-PEG NPs (with or without anti-CD7 antibody conjugation) with encapsulated EYFP mRNA. After

various incubation times, cells were recovered and the fluorescence analysed by flow cytometry. EYFP mRNA was encapsulated (1.5μg mRNA/mg of NPs; equivalent to 300ng of mRNA per well) in NPs modified by the inclusion of 5% (panel A) or 10% DOTAP (panel B) and incubated with A549-CD7 cells for 24, 48 or 72 hours. Fluorescence was measured by flow cytometry. Panel C, D: EYFP expression was further assessed from mRNA in DOTAP-NPs incubated with A549-CD7 for 24 hours with NP-DOTAP or i-NP-DOTAP (either 5%, panel C or 10% DOTAP, panel D) with increasing amounts of mRNA ranging from 75ng to 750 ng of mRNA per well.

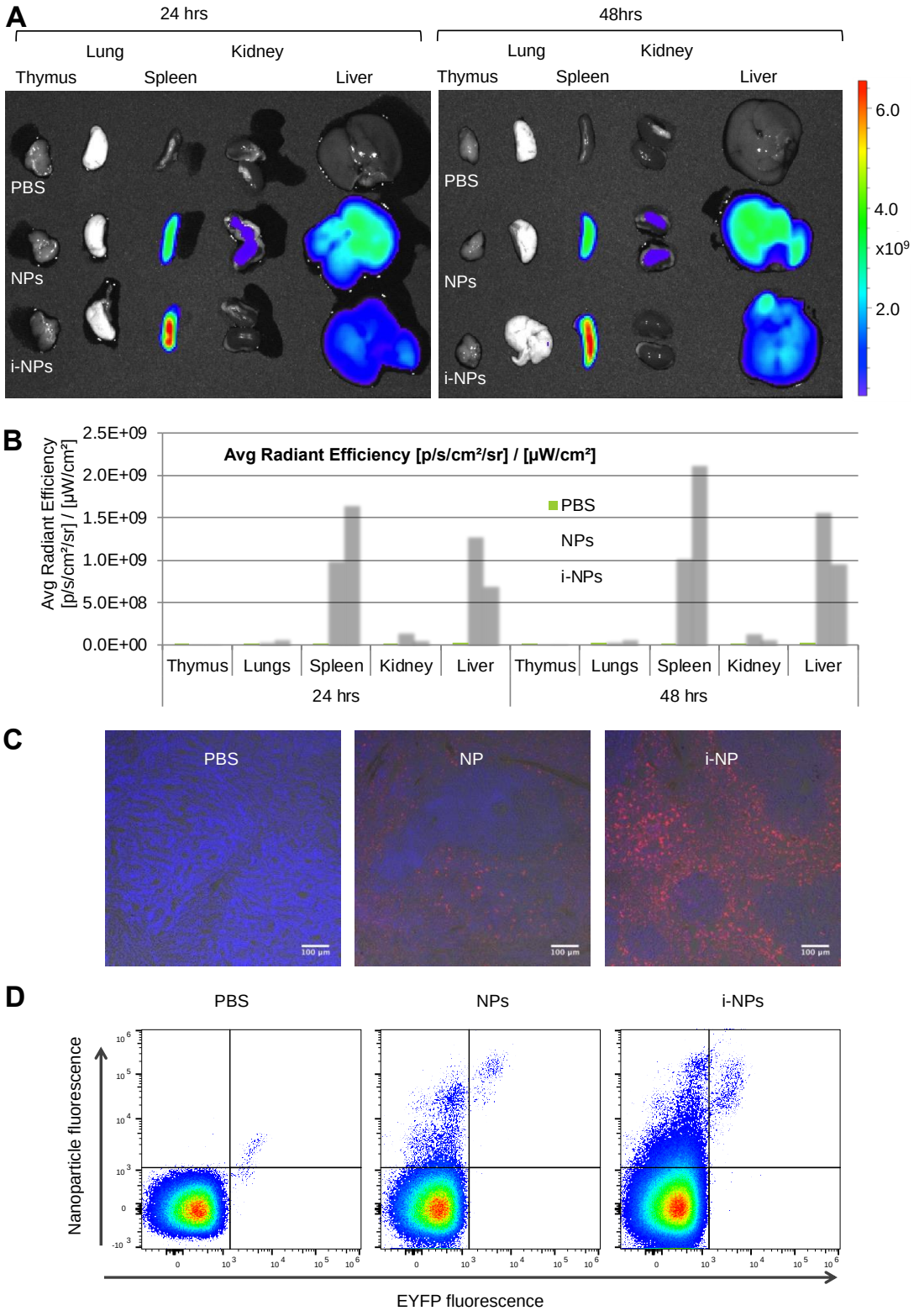

927

928 **Figure 6. *In vivo* biodistribution of i-NPs in transgenic mice expressing human**

929 **CD7**

930 Transgenic mice expressing human CD7 (Tg-hCD7) were injected (intravenous tail

931 vein) with 200µg of nanoparticles with encapsulated mRNA coding for EYFP and the

NPs were labelled with the near-IR fluorescent dye DiR. The NPs were with or without conjugated anti-CD7 antibody (respectively NPs or iNPs). Mice were sacrificed 24 and 48 hours after injection and the indicated, resected tissues were examined for fluorescence by the IVIS imaging (panel A). The quantification of the radiant efficiency of these organs, representing comparative deposition of the nanoparticles in various organs is given in panel B. Nanoparticle deposition in the spleens of the injected Tg-hCD7 mice was confirmed by histological examination of the spleens of injected mice sacrificed 24 hrs after intravenous administration of the nanoparticles. Spleens were fixed, sections made, stained with DAPI to highlight nuclei and examined for red fluorescence by confocal microscopy. Panel C shows sections of spleens from a Tg-HCD7 mouse injected with PBS only (left hand), with unconjugated nanoparticles (middle panel, NPs) or with conjugated nanoparticles (right hand panel, i-NPs). The expression from EYFP mRNA released and translated in spleen cells of injected Tg-hCD7 mice was analysed in mice sacrificed 48 hours after three intravenous administrations of the nanoparticles with encapsulated EYFP mRNA. Single cell suspensions were taken from spleens of mice and analysed by flow cytometry to determine EYFP fluorescence (x axis) and nanoparticle fluorescence (y axis). Panel D shows spleen cell flow cytometry data from Tg-hCD7 mice injected with PBS only (left hand panel), unconjugated nanoparticles (middle panel) or conjugated nanoparticles (right hand panel). The NPs were labelled with the near-IR fluorescent dye DiR.

The average radiant efficiency was based on [p/s/cm²/sr] / [µW/cm²]. The fluorescence bar is shown on the right in panel A.